Extended Data Figure 1: Characterization of the *Arabidopsis* transgenic lines.

From

NIK1-mediated translation suppression functions as a plant antiviral immunity mechanism

Cristiane Zorzatto, João Paulo B. Machado, Kênia V. G. Lopes, Kelly J. T. Nascimento, Welison A. Pereira, Otávio J. B. Brustolini, Pedro A. B. Reis, Iara P. Calil, Michihito Deguchi, Gilberto Sachetto-Martins, Bianca C. Gouveia, Virgílio A. P. Loriato, Marcos A. C. Silva, Fabyano F. Silva, Anésia A. Santos, Joanne Chory & Elizabeth P. B. Fontes

Nature **520**, 679–682 (30 April 2015) doi:10.1038/nature14171

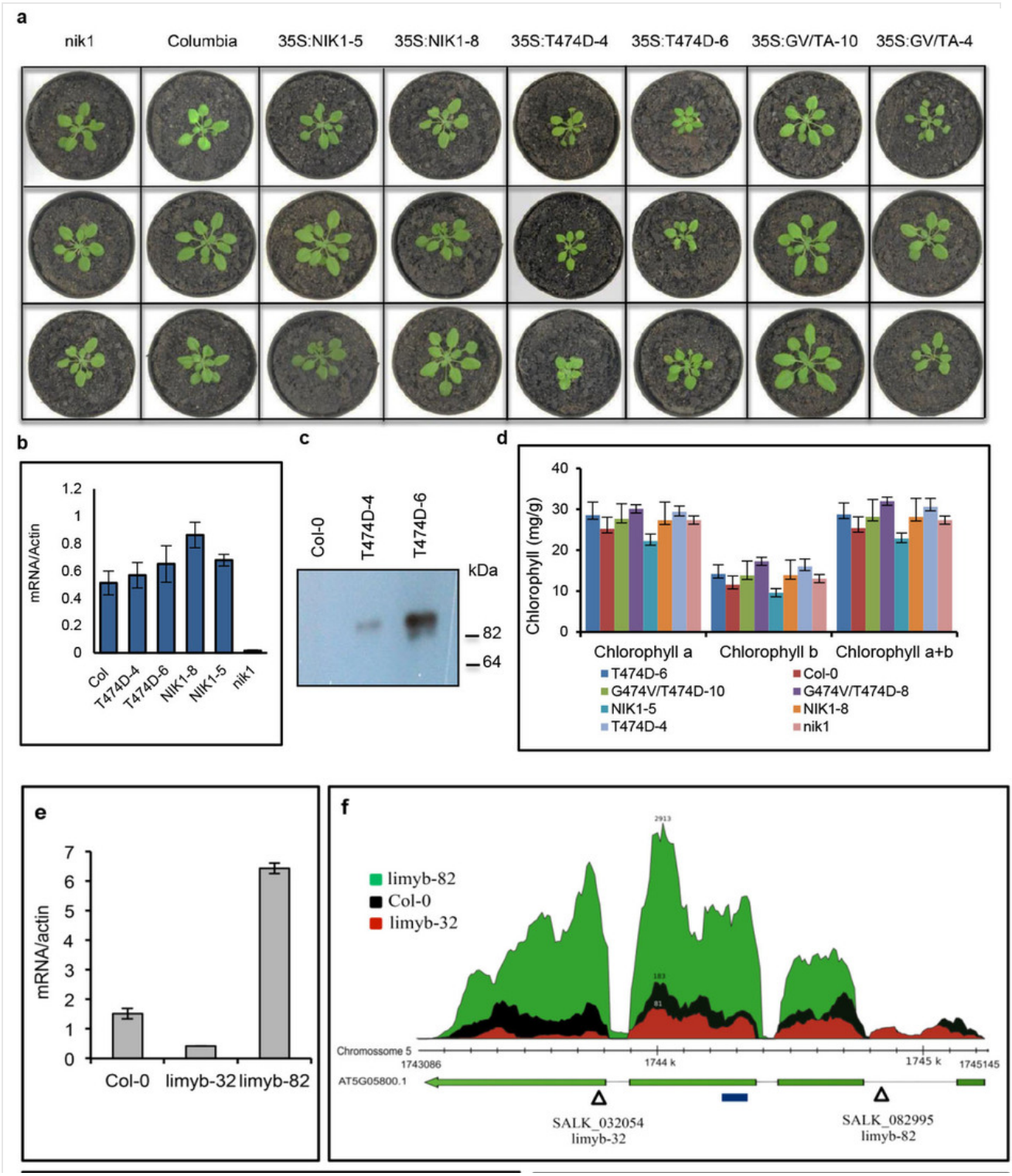

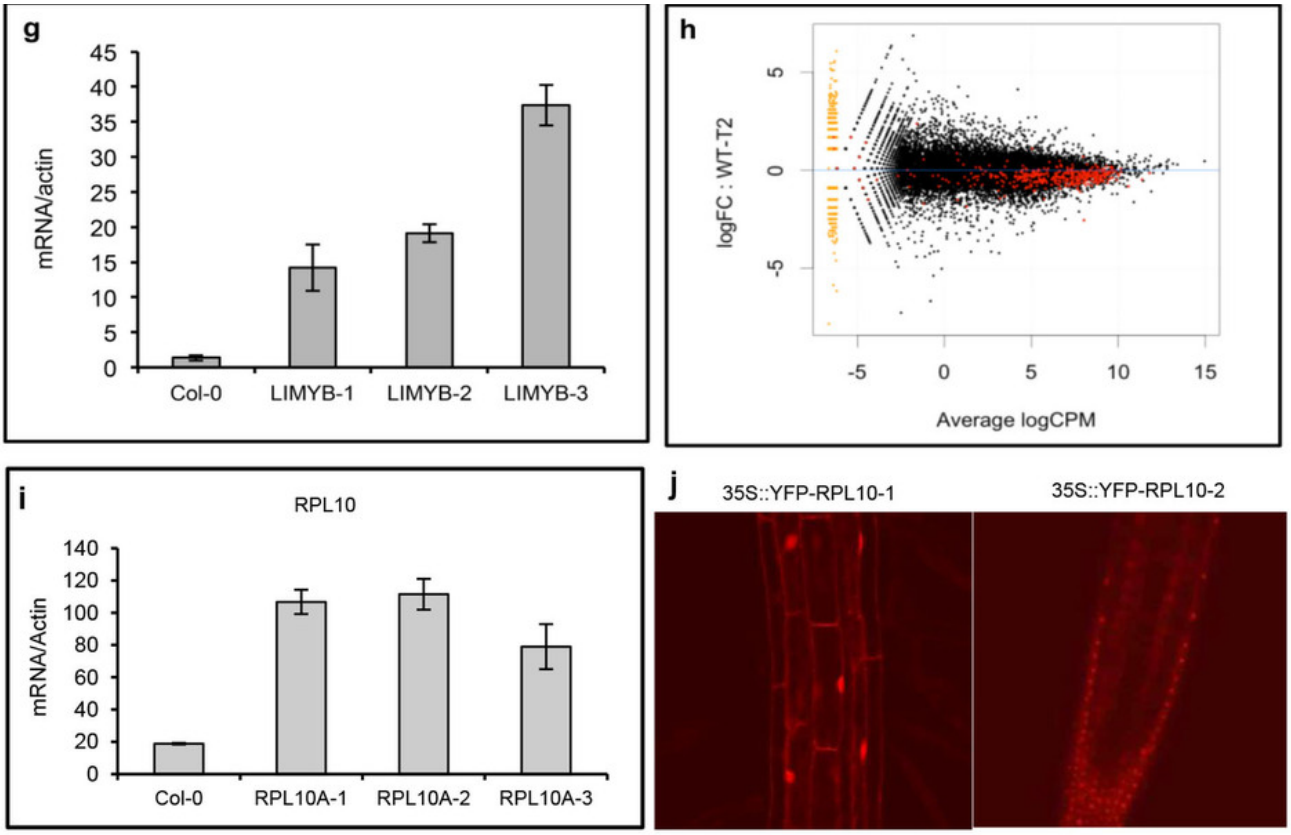

a, Phenotypes of wild-type (Col-0) and *nik1* plants transformed with NIK1 (NIK1-5 and NIK1-8), T474D (T474D-4 and T474D-6) or the double-mutant G4743V/T474A (inactive kinase, GV/TA-10 and GV/TA-4). Transgenic plants (R2 generation, $n = 15$) were grown in soil at 22 °C under short day conditions and photographed 2 weeks after planting. **b**, T474D transcript accumulation in transgenic lines (R2 generation). The expression of T474D or NIK1 in the leaves of independent transgenic lines was monitored by quantitative RT–PCR. Mean ± 95% confidence intervals ($n = 3$) based on bootstrap resampling replicates of three independent experiments. **c**, Accumulation of T474D–GFP in transgenic lines. Total protein was extracted from the leaves of independent transgenic lines (as indicated), immunoprecipitated and immunoblotted with an anti-GFP antiserum. **d**, Chlorophyll content of transgenic lines. Total chlorophyll, chlorophyll *a* and chlorophyll *b* were determined in leaf sectors of the indicated transgenic lines. Error bars, 95% confidence intervals ($n = 3$) based on bootstrap resampling replicates of four independent experiments. **e**, Transcript accumulation of *LIMYB* in T-DNA insertion mutant lines. *LIMYB* expression was monitored by qRT–PCR of RNA prepared from Col-0, *limyb-32* (SALk_032054) and *limyb-82* (SALK_082995) plants. Gene expression was calculated using the $2^{-\Delta Ct}$ method, and actin was used as an endogenous control. Error bars, 95% confidence intervals ($n = 3$) based on bootstrap resampling replicates of three independent experiments. **f**, Schematic representation of the *At5g05800* (*LIMYB*) locus in the chromosome 5 and RNA sequencing data. The *At5g05800* gene harbours three introns and four exons. Triangles show the positions of the T-DNA insertion in the *limyb-32* and *limyb-82* mutants, and the blue line indicates the position of the amplicon from **e**. The relative abundance of the mapped RNA hits in the *At5g05800* locus is shown in red in *limyb-32*, black in Col-0 and green in *limyb-82*. The accumulation of *LIMYB* transcripts was much lower in *limyb-32* and higher in *limyb-82* than in Col-0. Sequencing of the *limyb-32* and *limyb-82* transcripts revealed unprocessed intron sequences and premature stop codons that would have prevented the translation of a functional protein in these mutant lines. Therefore, *limyb-32* and *limyb-82* were confirmed as loss-of-function *limyb* mutant lines. **g**, *LIMYB* transcript accumulation in *LIMYB*-overexpressing lines (R2 generation). *LIMYB* expression in the leaves of independent transgenic lines was monitored by quantitative RT–PCR. Error bars, 95% confidence intervals ($n = 3$) based on bootstrap resampling replicates of three independent experiments. **h**, General downregulation of translational machinery-related genes in LIMYB-1 seedlings. The 'MA' plots show the log of the ratio of the expression levels against log concentration, and each dot represents a gene. This plot visualizes the contrast of LIMYB-1 and Col-0 seedlings. The smear of points on the left side indicates those genes that were observed in only one group of replicated samples, and the red points denote ribosomal and protein synthesis-related genes. CPM, counts per million; FC, fold change; WT, wild type. **i**, *RPL10* transcript accumulation in *RPL10*-overexpressing lines (R2 generation). The expression of an NLS-containing *RPL10* transgene in the leaves of independent transgenic lines was monitored by quantitative RT–PCR. Error bars, 95% confidence intervals ($n = 3$) based on bootstrap resampling replicates of three independent experiments. **j**, Nuclear localization of the NLS-containing YFP–RPL10 fusion in transgenic lines. Root tips from transgenic seedlings expressing the NLS-containing YFP–RPL10 fusion were directly examined under a laser confocal microscope. The figure shows representative confocal images from five independent biological replicates.

Nature ISSN 0028-0836 EISSN 1476-4687

© 2015 Macmillan Publishers Limited. All Rights Reserved.
partner of AGORA, HINARI, OARE, INASP, ORCID, CrossRef, COUNTER and COPE

Extended Data Figure 2: Expression of immune-system-related genes in T474D-overexpressing lines and in *LIMYB*-overexpressing lines.

From

NIK1-mediated translation suppression functions as a plant antiviral immunity mechanism

Cristiane Zorzatto, João Paulo B. Machado, Kênia V. G. Lopes, Kelly J. T. Nascimento, Welison A. Pereira, Otávio J. B. Brustolini, Pedro A. B. Reis, Iara P. Calil, Michihito Deguchi, Gilberto Sachetto-Martins, Bianca C. Gouveia, Virgílio A. P. Loriato, Marcos A. C. Silva, Fabyano F. Silva, Anésia A. Santos, Joanne Chory & Elizabeth P. B. Fontes

Nature **520**, 679–682 (30 April 2015) doi:10.1038/nature14171

a

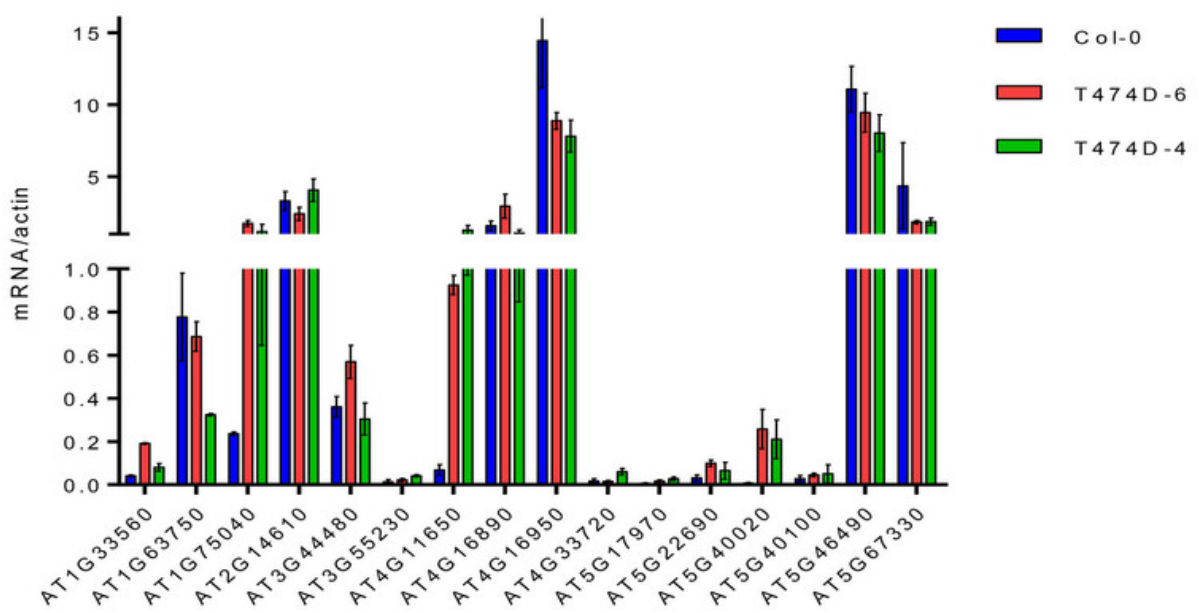

b

TAIR 10	log2 (Fold Change)	q-value (FDR)	Symbol	Description
AT2G14610.1	-2.0266	0.00166622880245705	PR1	Pathogenesis-related gene 1
AT4G11650.1	-1.4957	0.00338420995139227	OSM34	Osmotin 34
AT3G44480.1	-0.1045	0.763775753084199	RPP1, cog1	Disease resistance protein (TIR-NBS-LRR class)
AT4G16890.1	-0.0927	0.81956561493713	SNC1, BAL	Suppressor of NPR1
AT4G16950.1	-0.0397	0.923791385238997	RPP5	Disease resistance protein (TIR-NBS-LRR class)
AT4G33720.1	0.0	0.0	PR1	Pathogenesis-related 1 protein
AT5G17970.1	0.0	0.0		Disease resistance protein (TIR-NBS-LRR class)
AT5G40100.1	0.1313	1		Disease resistance protein (TIR-NBS-LRR class)
AT5G46490.1	0.2537	0.557766109000824		Disease resistance protein (TIR-NBS-LRR class)
AT5G67330.1	0.3322	0.497337654351076	NRAMP4	Natural resistance associated macrophage protein 4
AT3G55230.1	0.8647	0.293804289942712		Disease resistance-responsive (dirigent-like protein)
AT5G40020.1	1.1202	0.360825407950067		Pathogenesis-related thaumatin superfamily protein
AT1G63750.1	1.2229	0.209031413356128		Disease resistance protein (TIR-NBS-LRR class)
AT1G33560.1	1.3284	0.0253419904795418	ADR1	Disease resistance protein (CC-NBS-LRR class)
AT5G22690.1	1.8197	0.0106685101569183		Disease resistance protein (TIR-NBS-LRR class)
AT1G75040.1	2.8732	0.000722106289807284	PR-5	Pathogenesis-related gene 5

c

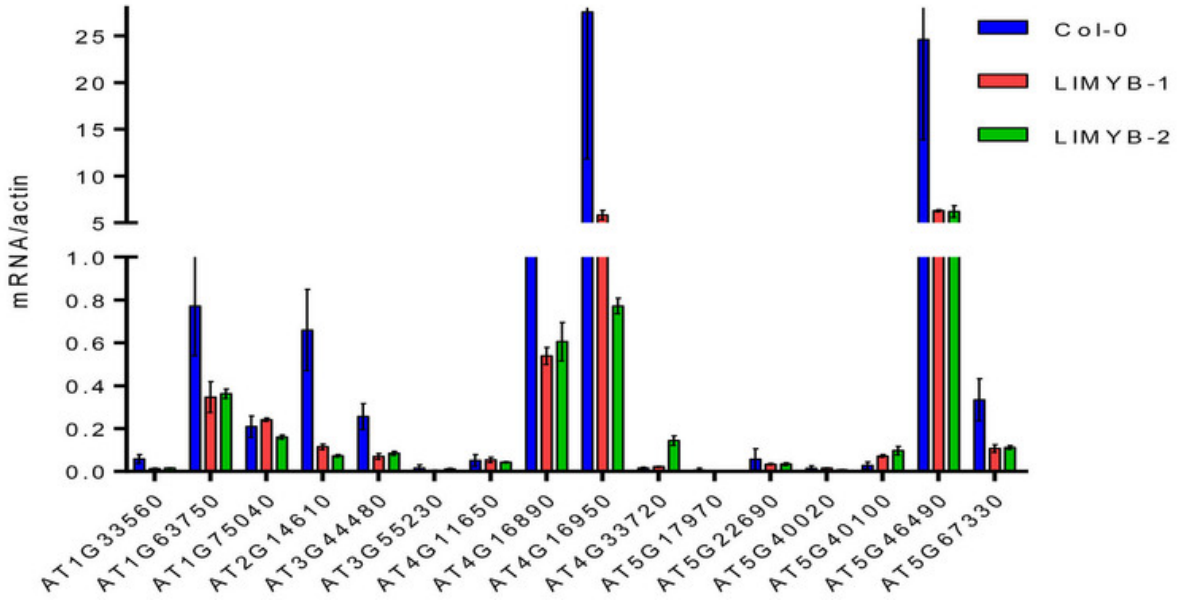

a–**c**, On the basis of our global comparison of EST sequences (Fig. 1a) and the role of NIK as an antiviral receptor, we asked whether the constitutive activation of NIK would elicit a defence response similar to that induced by geminivirus infection via the salicylic acid pathway or typical defence responses to

virus. No significant gene enrichment was detected in the virus-induced gene silencing (GO:0009616) and viral defence response (GO:0051607) categories using the gene set enrichment analysis (GSEA) method (Supplementary Table 2). For the immune system category, gene enrichment was found in both up- and downregulated changes using the GSEA method. However, the typical markers of salicylic acid signalling, such as *PR1* and *SNC1*, were either non-differentially expressed or downregulated, and the expression of T474D did not enhance the salicylic acid level in the transgenic lines. Collectively, these results indicate that ectopic expression of T474D did not activate typical viral defences, such as salicylic acid signalling or gene silencing. **a**, **b**, Transcript accumulation of selected immune-system-related gene markers by RT–PCR (**a**) or RNA-sequencing in T474D-overexpressing lines (**b**). qRT–PCR of a representative sample confirmed an 80% match with the RNA-sequencing results. **c**, Transcript accumulation of the immune-system-related genes in LIMYB-overexpressing lines. The expression of the indicated genes in the leaves of independent transgenic lines was monitored by qRT–PCR. **a**, **c**, Mean ± 95% confidence intervals (n = 3) are shown, based on bootstrap resampling replicates of three independent experiments.

Nature ISSN 0028-0836 EISSN 1476-4687

© 2015 Macmillan Publishers Limited. All Rights Reserved.
partner of AGORA, HINARI, OARE, INASP, ORCID, CrossRef, COUNTER and COPE

Extended Data Figure 3: Ectopic expression of T474D-D downregulates translational-machinery-related genes and suppresses *de novo* protein synthesis.

From

NIK1-mediated translation suppression functions as a plant antiviral immunity mechanism

Cristiane Zorzatto, João Paulo B. Machado, Kênia V. G. Lopes, Kelly J. T. Nascimento, Welison A. Pereira, Otávio J. B. Brustolini, Pedro A. B. Reis, Iara P. Calil, Michihito Deguchi, Gilberto Sachetto-Martins, Bianca C. Gouveia, Virgílio A. P. Loriato, Marcos A. C. Silva, Fabyano F. Silva, Anésia A. Santos, Joanne Chory & Elizabeth P. B. Fontes

Nature **520**, 679–682 (30 April 2015) doi:10.1038/nature14171

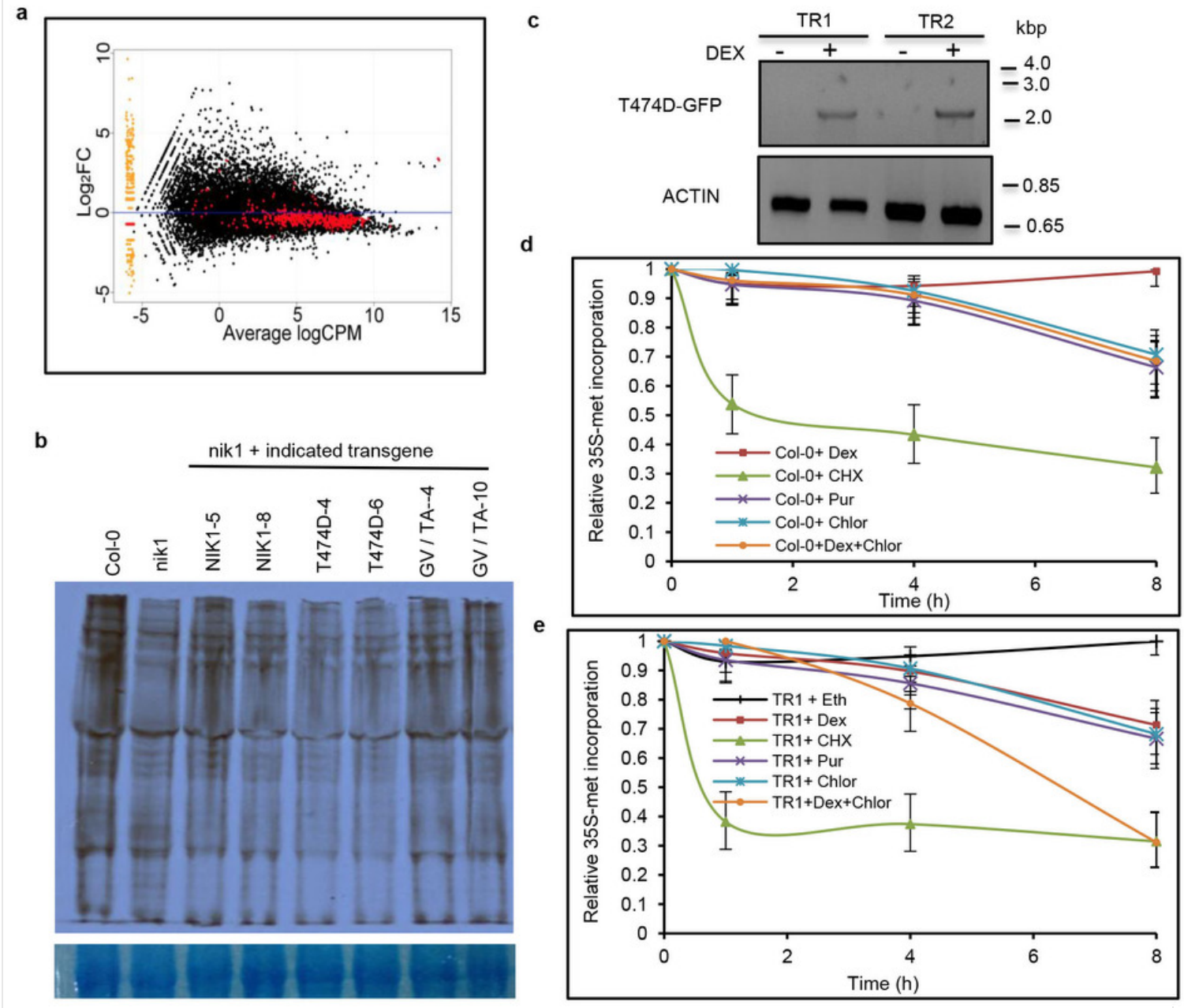

a, Representation of the translational-machinery-related genes differentially expressed in the T474D lines. The 'MA' plots show the log of the ratio of expression levels versus the log concentration, and each dot represents a gene. This plot represents the contrast between the T474D mock-inoculated lines

and the Col-0 mock-inoculated lines. The red points denote ribosomal and protein synthesis-related genes (as shown in Supplementary Table 3). **b**, Downregulation of global translation by ectopic expression of T474D in *Arabidopsis*. The *in vivo* labelling of leaf proteins with [^{35}S]Met was performed in 20-day-old Col-0 plants and T474D transgenic lines. The total protein extracts were fractionated by SDS–polyacrylamide gel electrophoresis (SDS–PAGE), and the radioactive bands were quantified by densitometric analysis of the images obtained by autoradiography. The labelling percentage was normalized to the leaf chlorophyll content, and the protein loading on the gel was adjusted to the Coomassie-stained band of the large subunit of rubisco. **c**, Induction of T474D expression by dexamethasone (DEX) in *Arabidopsis* transgenic seedlings. The constitutive expression of T474D was associated with stunted growth in the transgenic lines (Extended Data Fig. 1a) and repression of global protein synthesis (Fig. 1b). These phenotypes precluded the use of an appropriate normalization method for protein loading in comparative gels of contrasting genotypes to estimate precisely the T474D-mediated protein synthesis inhibition in our assay. To overcome this limitation, we used a dexamethasone-inducible promoter to control the T474D expression in the transgenic lines. *Arabidopsis* seedlings independently transformed with a T474D–GFP fusion under the control of a dexamethasone-inducible promoter (TR1 and TR2) were treated with 30 μM dexamethasone for 8 h, and the induction of T474D–GFP expression was monitored by semi-quantitative RT–PCR. The dexamethasone-induced expression of T474D for 8 h led to a higher inhibition of *de novo* protein synthesis in the transgenic lines, as measured by TCA-precipitable radioactivity, which could be normalized to total protein (TR1 and TR2; Fig. 1c). **d**, Inhibition of *de novo* protein synthesis by protein synthesis inhibitors in Col-0, untransformed lines. We also compared the T474D-mediated suppression of translation with known global translation inhibitors, such as the cytosolic protein synthesis inhibitors cycloheximide and puromycin and the chloroplast translation suppressor chloramphenicol. *Arabidopsis* seedlings (10 days old) were treated with 10 μM cycloheximide (Cyclo), 10 μM puromycin (Pur), 25 μM chloramphenicol (Chlor) or 30 μM dexamethasone (Dex) for the indicated periods of time, and then they were pulse labelled with L-[^{35}S]Met for 60 min. Lysates of treated cells were measured by liquid scintillation counting and normalized to total protein. The relative [^{35}S]Met incorporation was normalized to wild-type (WT = 1) control without treatment. Means ± 95% confidence intervals (n = 3) based on bootstrap resampling replicates of three independent experiments are shown. **e**, Inhibition of *de novo* protein synthesis by inducible expression of T474D. Seedlings (10 days old) from the TR1 transgenic line were treated with dexamethasone and the protein synthesis inhibitors for the times as indicated in the figure, and then they were pulse labelled with L-[^{35}S]Met for 60 min. Lysates were processed as described in **d**. Means ± 95% confidence interval (n = 3) based on bootstrap resampling replicates of three independent experiments are shown. Cycloheximide was the most effective inhibitor of translation in both the wild-type and T474D-expressing lines. T474D expression inhibited global translation to the same extent as puromycin and caused a further inhibition in the level of chloramphenicol translational inhibition in a combined treatment. The increase in translational inhibition by combining T474D expression and chloramphenicol treatment may indicate that T474D inhibits cytosolic protein synthesis, which is consistent with the T474D-mediated downregulation of components of the cytosolic translational machinery (Supplementary Table 3).

Nature ISSN 0028-0836 EISSN 1476-4687

© 2015 Macmillan Publishers Limited. All Rights Reserved.
partner of AGORA, HINARI, OARE, INASP, ORCID, CrossRef, COUNTER and COPE

Extended Data Figure 4: Isolation of PS fractions from *Arabidopsis* seedlings and LIMYB-mediated inhibition of protein synthesis.

From

NIK1-mediated translation suppression functions as a plant antiviral immunity mechanism

Cristiane Zorzatto, João Paulo B. Machado, Kênia V. G. Lopes, Kelly J. T. Nascimento, Welison A. Pereira, Otávio J. B. Brustolini, Pedro A. B. Reis, Iara P. Calil, Michihito Deguchi, Gilberto Sachetto-Martins, Bianca C. Gouveia, Virgílio A. P. Loriato, Marcos A. C. Silva, Fabyano F. Silva, Anésia A. Santos, Joanne Chory & Elizabeth P. B. Fontes

Nature **520**, 679–682 (30 April 2015) doi:10.1038/nature14171

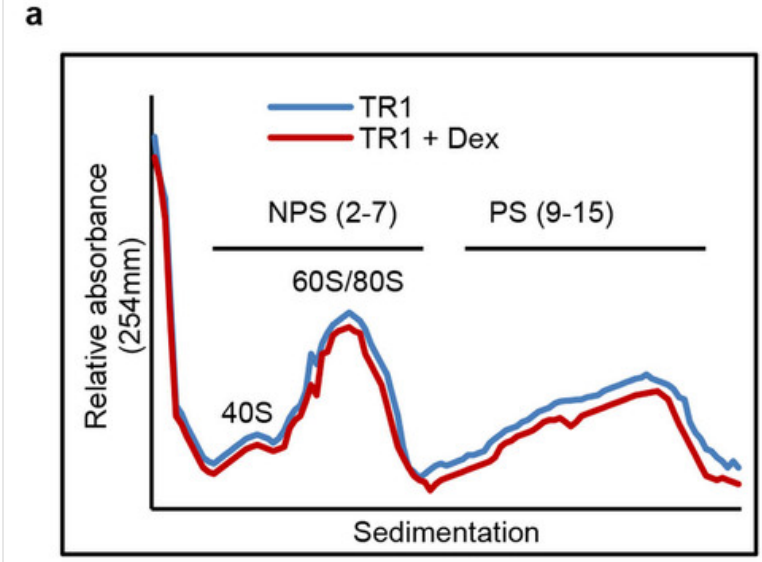

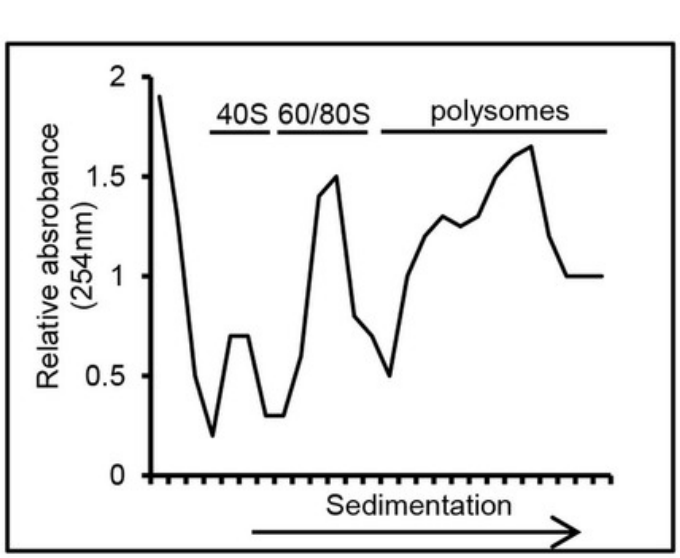

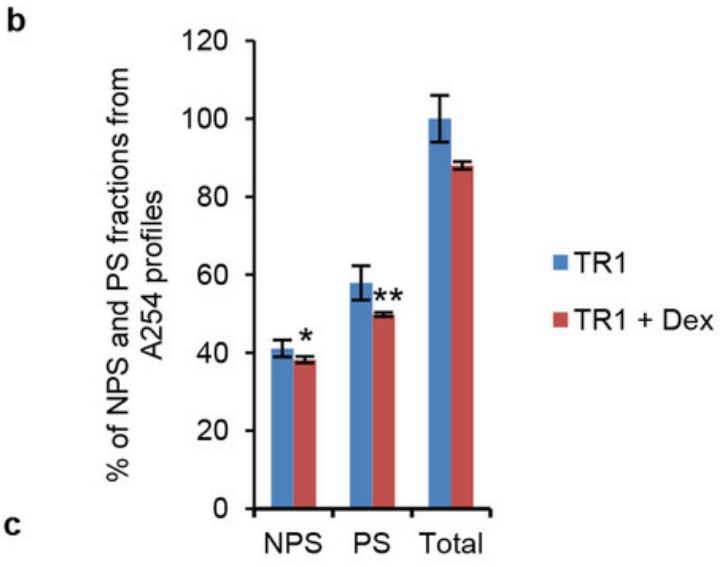

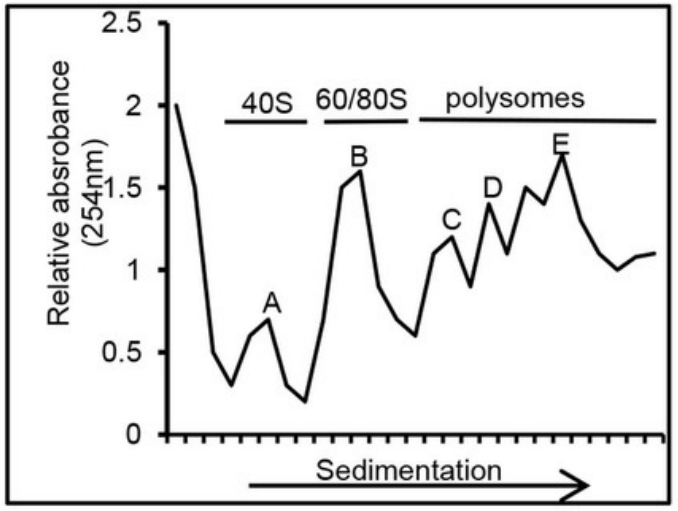

c

Relative RNA content in NPS and PS complexes

	NPS	PS	Total
TR1	0.45 ± 0.03	0.55 ± 0.02	100%
TR1+ Dex	0.39 ± 0.02	0.48 ± 0.02	87%

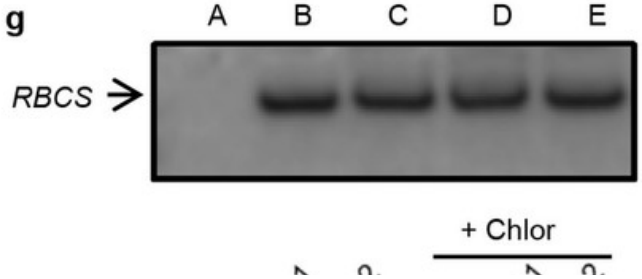

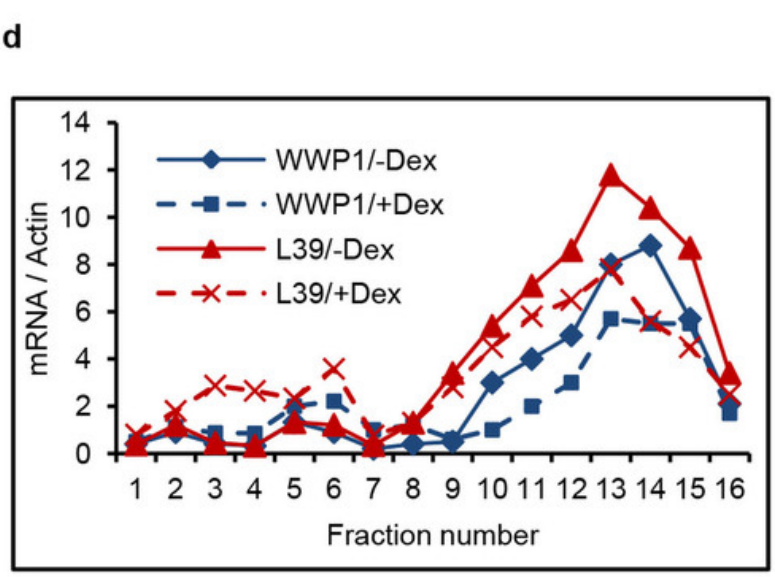

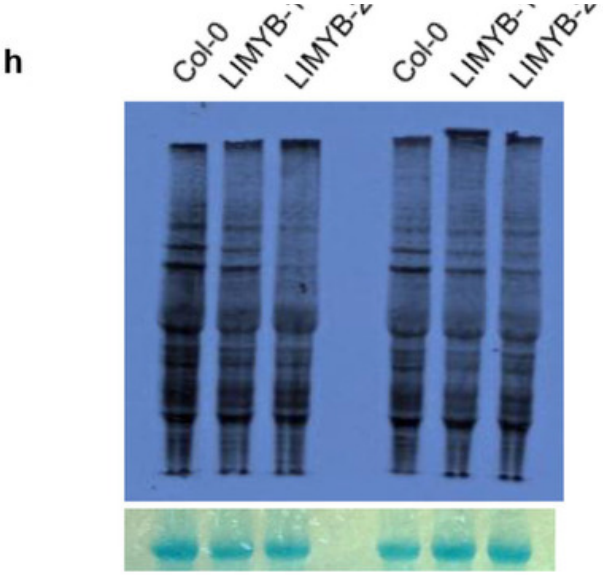

a, Ultraviolet absorbance profiles of the sucrose gradient used for RNA fractionation of dexamethasone (Dex)-inducible T474D transgenic lines. Sixteen fractions of 310 µl were collected. NPS RNA includes complexes ≤ 80S that fractionated in the top half of the gradient (fractions 2–7) and PS (polysome) represents complexes fractionated in the bottom of the gradient (fractions 9–15). **b**, Distribution (%) of NPS and PS fractions on polysome density gradients. The percentage of NPS or PS was calculated by integrating the areas under the corresponding peaks in the $A_{254\ nm}$ profile delimited by a gradient baseline absorbance (buffer density). Values are the average ± standard deviation (s.d.) of three biological replicates. NPS and PS fractions from T474D + Dex samples were significantly different from the corresponding fractions of the T474D samples by the *t*-test (greater). NPS, *P* value = 0.03725; PS, *P* value = 0.009137 (*t*-test; greater). **c**, Relative RNA content in NPS and PS complexes. RNA was precipitated from NPS and PS density regions of sucrose gradients (as in **a**) and quantified. Relative NPS RNA and PS RNA contents from T474D and T474D + Dex samples were calculated in relation to the total NPS + PS content from T474D. Values for the relative NPS and PS RNA content are the average ± s.d. of three biological replicates and they were significantly different between the samples ($P < 0.01$, *t*-test). **d**, Distribution of specific mRNAs in the PS gradient fractions from extracts prepared from T474D seedlings treated (or not) with dexamethasone. The RNA on each fraction was reverse transcribed and aliquots amplified with specific primers for the indicated genes by qPCR. **e**, Ultraviolet absorbance profiles of the sucrose gradient used for the RNA fractionation of Col-0 seedlings. PSs from 15-day-old Col-0 seedlings were fractionated on a sucrose gradient, and the fractions were manually collected. **f**, Ultraviolet absorbance profiles of the sucrose gradient used for RNA fractionation from T474D seedlings. PSs from 15-day-old T474D-overexpressing seedlings were fractionated on a sucrose gradient, and the fractions were manually collected. **g**, Levels of the small subunit of rubisco (*RBCS*) mRNA per fraction. The levels of mRNA of *RBCS* were examined by northern blotting. This control was used to ensure the quality and distribution of a specific mRNA. **h**, Overexpression of LIMYB suppresses cytosolic translation. *In vivo* labelling of leaf proteins with [^{35}S]Met was performed in Col-0 and *LIMYB-1* transgenic seedlings in the presence and absence of chloramphenicol treatment. The total protein extracts were fractionated by SDS–PAGE, and the radioactive bands were quantified by densitometric analysis of the images obtained by autoradiography. The labelling percentage was normalized to the leaf chlorophyll content, and protein loading is shown by Coomassie staining of the radioactive gel.

Nature ISSN 0028-0836 EISSN 1476-4687

© 2015 Macmillan Publishers Limited. All Rights Reserved.
partner of AGORA, HINARI, OARE, INASP, ORCID, CrossRef, COUNTER and COPE

Extended Data Figure 5: Ectopic expression of T474D and LIMYB confers tolerance to begomovirus infection.

From

NIK1-mediated translation suppression functions as a plant antiviral immunity mechanism

Cristiane Zorzatto, João Paulo B. Machado, Kênia V. G. Lopes, Kelly J. T. Nascimento, Welison A. Pereira, Otávio J. B. Brustolini, Pedro A. B. Reis, Iara P. Calil, Michihito Deguchi, Gilberto Sachetto-Martins, Bianca C. Gouveia, Virgílio A. P. Loriato, Marcos A. C. Silva, Fabyano F. Silva, Anésia A. Santos, Joanne Chory & Elizabeth P. B. Fontes

Nature **520**, 679–682 (30 April 2015) doi:10.1038/nature14171

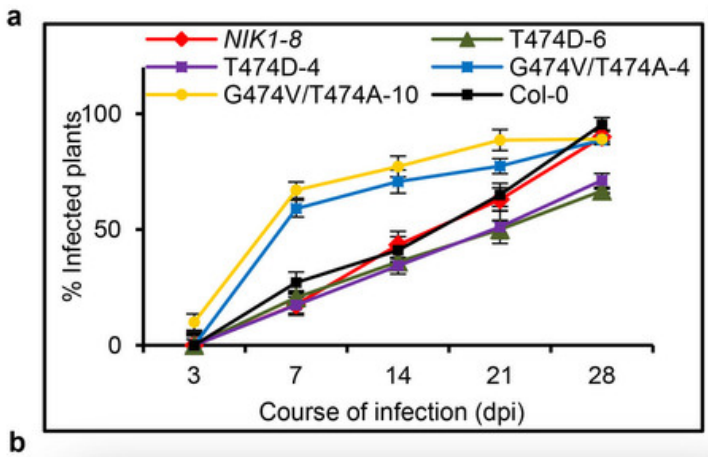

c

T474D infected – Col-0 infected (10 days)			
Viral Component	log2FC	q-value	NCBI Locus ID
A	0.9139909	1.381925e-01*	CLU65529
B	1.2348528	1.257184e-08	CLU65530
T474D infected – WT infected (21 days)			
Viral Component	log2FC	q-value	NCBI Locus ID
A	-4.534558	7.640602e-126	CLU65529
B	-3.682993	1.129406e-112	CLU65530

*Non significative according to Negative Binomial Exact Test (edgeR) by q-value (FDR) < 0.05

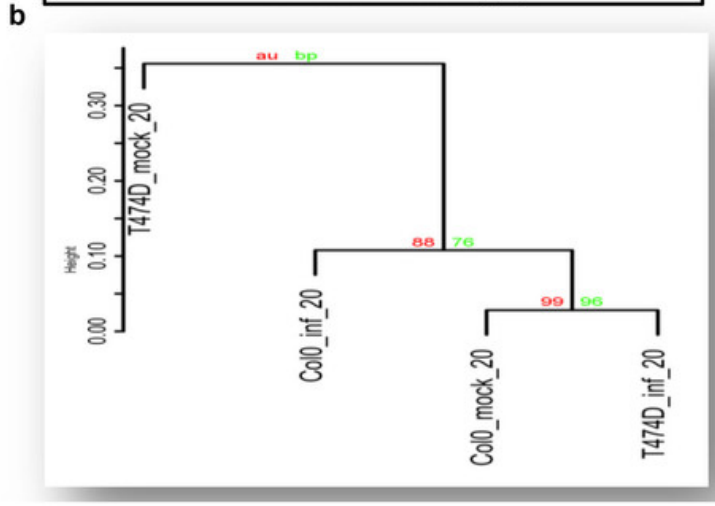

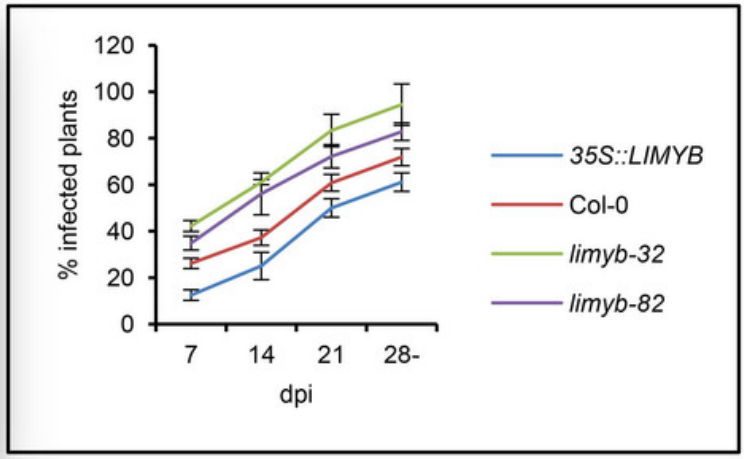

a, Delayed onset of infection in the T474D-4- and T474D-6-overexpressing lines. Ecotype Col-0 plants, as well as the T474D-4- and T474D-6-overexpressing lines, and the *NIK1-8* and G473V/T474A-overexpressing lines were infected with CaLCuV DNA by the biolistic method. The progression of the infection was monitored by PCR detection of viral DNA in the systemic leaves of the inoculated plants. The values represent the percentages of systemically infected plants at different dpi. Error bars, 95% confidence intervals (n = 3) based on bootstrap resampling replicates of four independent experiments. **b**, Upon symptom development, the T474D-induced transcriptome diverges from the infected Col-0 transcriptome. The mock-inoculated T474D-overexpressing lines exhibited a constitutively infected wild-type transcriptome at 10 dpi (Fig. 1a). Nevertheless, these T474D transgenic lines did not phenocopy the infected wild-type plants because they did not develop symptoms of viral infection. In fact, the wild-type plants displayed typical symptoms of CaLCuV infection at 21 dpi, such as leaf distortion, stunting with epinasty and chlorosis (Fig. 1e). The symptoms in the T474D-expressing lines at 21 dpi, however, were greatly attenuated, with no visible leaf distortion or chlorosis. To examine these phenotypes, we performed a Ward hierarchical clustering of the gene expression data (normalized by the trimmed mean of *M*-values (TMM) normalization method) from the *Arabidopsis* infection experiments at 21 dpi. The TMM normalization method assumes that the majority of genes are not differentially expressed, and it adjusts genes with larger read counts and lower variance on the logarithmic scale. The dendrogram provides two types of *P* values: AU (black) and BP (grey). The AU *P* value comes from multiscale bootstrap resampling, while the BP value represents normal bootstrap resampling. These *P* values were calculated by multiscale bootstrap resampling using the R-cran package pvclust with a cut-off of 0.05. These *P* values show the significance of the proximity of each gene expression experiment profile. The cluster analysis at 21 dpi indicated that when symptoms had developed in the infected Col-0 leaves, the T474D-induced transcriptome diverged from the infected Col-0 transcriptome. The mock T474D

transcriptome formed a unique clade, while the infected T474D transcriptome was more closely related to the mock-inoculated Col-0 transcriptome. **c**, Reduced viral transcript accumulation in T474D-overexpressing lines at 21 dpi. RNA-sequencing data of viral gene transcripts in the systemic leaves of infected wild-type and T474D-overexpressing plants at 10 dpi and 21 dpi. **d**, The onset of infection is delayed in *LIMYB*-overexpressing lines. Ecotype Col-0 plants and *LIMYB*-overexpressing and *limyb* mutant lines were infected with CaLCuV DNA using the biolistic method. The progression of the infection was monitored by the PCR detection of viral DNA in the systemic leaves of the inoculated plants. The values represent the percentages of systemically infected plants at different dpi. Error bars, 95% confidence intervals (n = 3) based on bootstrap resampling replicates of four independent experiments.

Nature ISSN 0028-0836 EISSN 1476-4687

© 2015 Macmillan Publishers Limited. All Rights Reserved.
partner of AGORA, HINARI, OARE, INASP, ORCID, CrossRef, COUNTER and COPE

Extended Data Figure 6: LIMYB, which belongs to the MYB domain-containing superfamily, interacts with RPL10 in the yeast two-hybrid system.

From

NIK1-mediated translation suppression functions as a plant antiviral immunity mechanism

Cristiane Zorzatto, João Paulo B. Machado, Kênia V. G. Lopes, Kelly J. T. Nascimento, Welison A. Pereira, Otávio J. B. Brustolini, Pedro A. B. Reis, Iara P. Calil, Michihito Deguchi, Gilberto Sachetto-Martins, Bianca C. Gouveia, Virgílio A. P. Loriato, Marcos A. C. Silva, Fabyano F. Silva, Anésia A. Santos, Joanne Chory & Elizabeth P. B. Fontes

Nature **520**, 679–682 (30 April 2015) doi:10.1038/nature14171

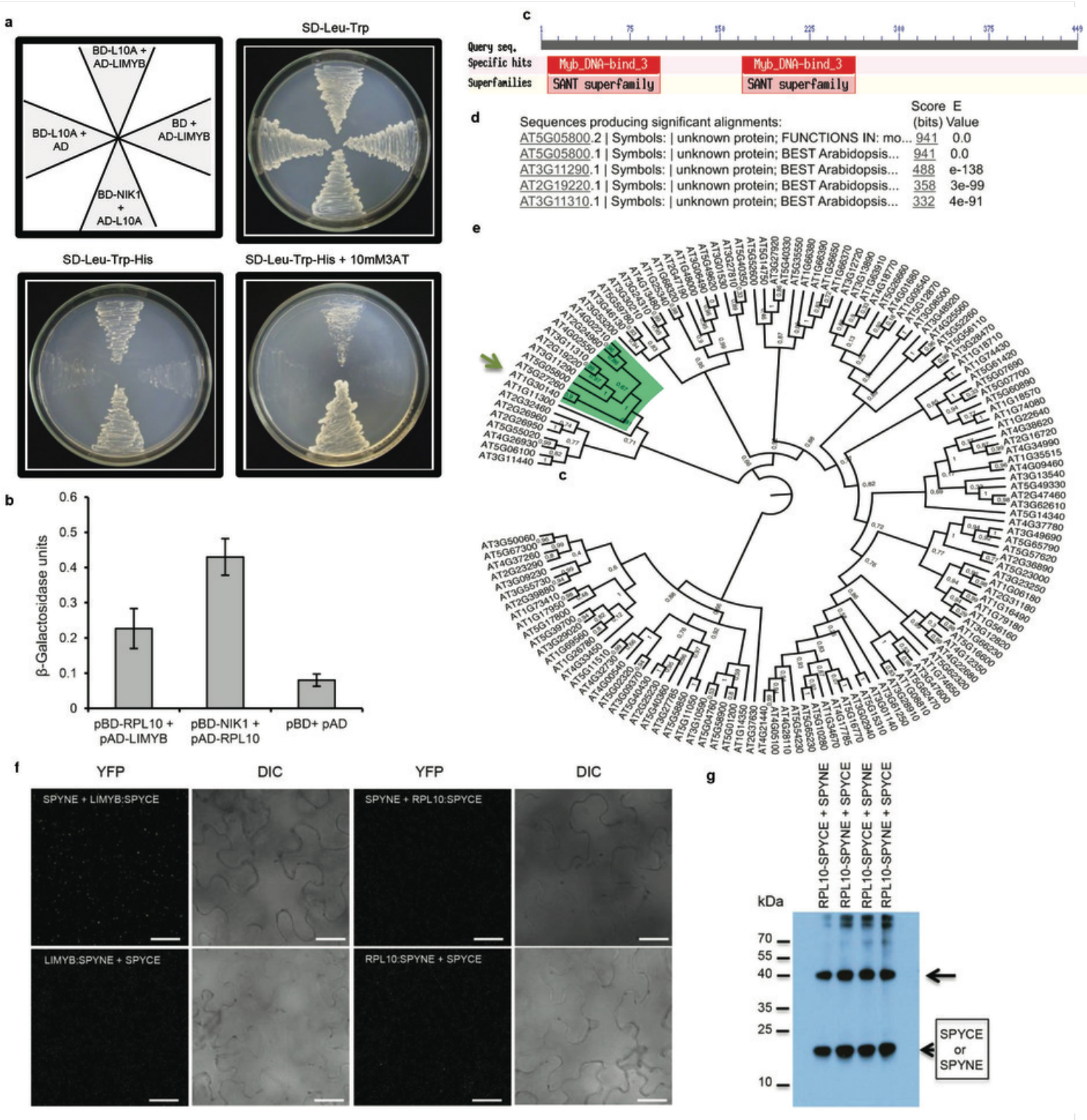

a, LIMYB and RPL10 interact in yeast. LIMYB was expressed in yeast as a GAL4 activation domain (AD) fusion (pAD–LIMYB), and RPL10 was expressed as a GAL4 binding domain (BD) fusion (pBD–RPL10). The interactions between the tested proteins were examined by monitoring His prototrophy. **b**, The interactions were further confirmed by measuring the expression activity of the β-galactosidase reporter enzyme for the second reporter gene, β-galactosidase. The interaction between pAD–RPL10 and pBD–NIK1 was monitored as a positive control. Means ± 95% confidence intervals (n = 3) based on bootstrap resampling replicates of three technical replicates are shown. **c**, LIMYB harbours two MYB domains. The position of these MYB domains is indicated in the schematic representation of the LIMYB primary structure. **d**, Sequence identity of the closest related *LIMYB* (*At5g05800*) homologues. **e**, Dendrogram of MYB domain-containing proteins from *Arabidopsis*. The MYB family sequences were retrieved from the Agris database (http://arabidopsis.med.ohio-state.edu). The alignment was performed by Maft aligner software using full-length sequences, and the tree was built by Fasttree software (the bootstrap values are indicated close to the branch divisions). The arrow indicates *LIMYB* (*At5g05800*). **f**, **g**, The negative controls used in the BiFC analysis. **f**, Confocal fluorescent image of SPYNE + LIMYB:SPYCE, LIMYB:SPYNE + SPYCE, SPYNE + RPL10:SPYCE and RPL10:SPYNE + SPYCE, as indicated in the figure. We used a BiFC assay to determine whether RPL10 and LIMYB interact in the nuclei of plant cells. The formation of a RPL10–LIMYB complex occurred in the nuclei of transfected cells independent of the orientation of the LIMYB or RPL10 fusions (amino terminus or carboxy terminus of YFP; Fig. 2a), and the reconstituted

fluorescent signal was much higher than that of the background (control panels with combinations of the protein fusions with empty vectors). The figure displays representative samples from three independent biological repeats. Scale bars, 20 μm. **g**, The C-terminal (SPYCE) and N-terminal region (SPYNE) of YFP accumulates detectably in co-transfected leaves. Total protein extracts from leaves co-transfected with the indicated constructs were immunoblotted with anti-YFP serum. The arrow indicates the position of RPL10–SPYCE and RPL10–SPYNE fusions, and arrowheads indicate the positions of the C-terminal (SYYCE) and N-terminal (SPYNE) regions of YFP.

Nature ISSN 0028-0836 EISSN 1476-4687

© 2015 Macmillan Publishers Limited. All Rights Reserved.
partner of AGORA, HINARI, OARE, INASP, ORCID, CrossRef, COUNTER and COPE

Extended Data Figure 7: Nuclear localization of LIMYB.

From

NIK1-mediated translation suppression functions as a plant antiviral immunity mechanism

Cristiane Zorzatto, João Paulo B. Machado, Kênia V. G. Lopes, Kelly J. T. Nascimento, Welison A. Pereira, Otávio J. B. Brustolini, Pedro A. B. Reis, Iara P. Calil, Michihito Deguchi, Gilberto Sachetto-Martins, Bianca C. Gouveia, Virgílio A. P. Loriato, Marcos A. C. Silva, Fabyano F. Silva, Anésia A. Santos, Joanne Chory & Elizabeth P. B. Fontes

Nature **520**, 679–682 (30 April 2015) doi:10.1038/nature14171

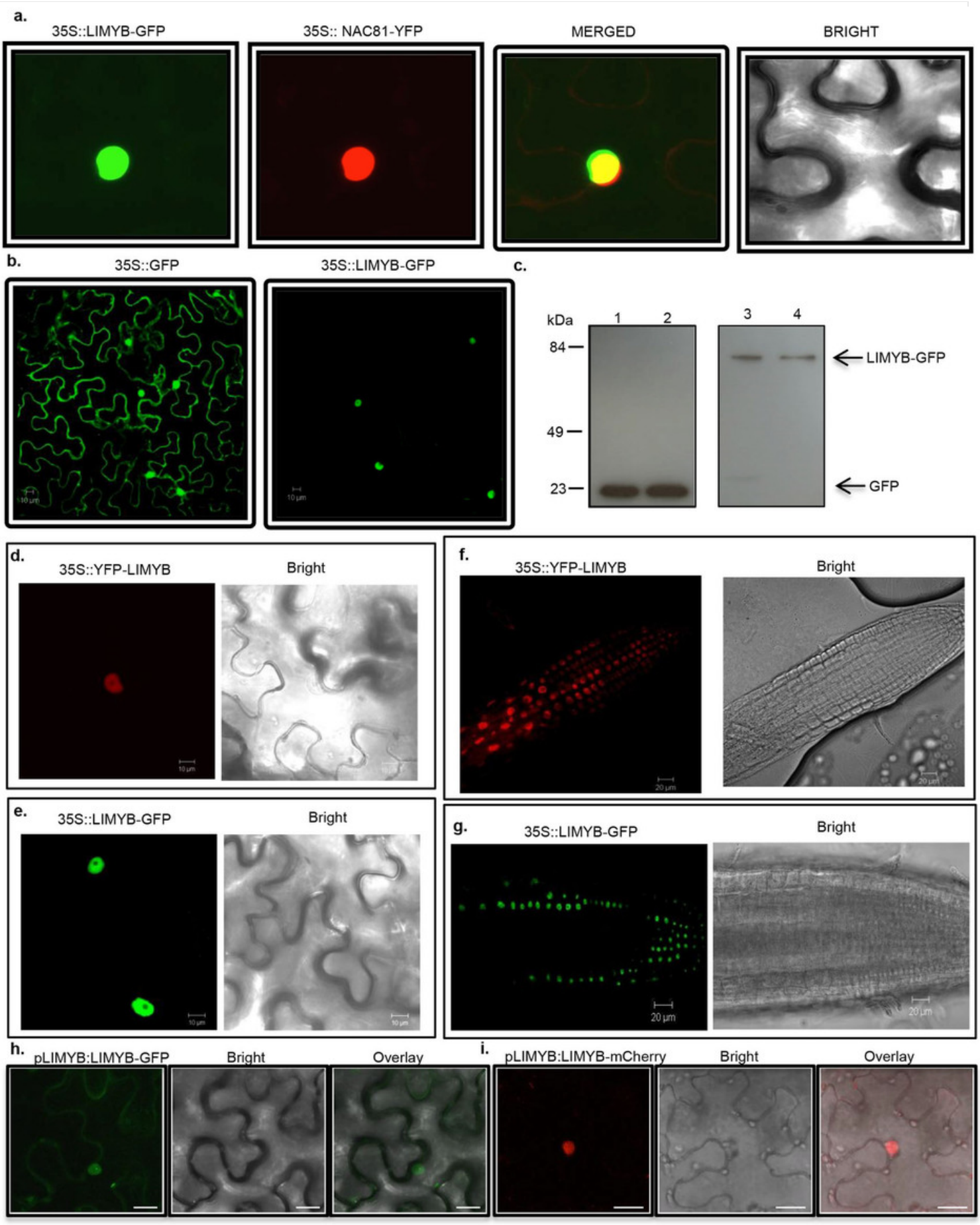

a, Colocalization of LIMYB with the nuclear marker gene *Glycine max* (*Gm*)*NAC81*. *N. benthamiana* leaves were co-infiltrated with *A. tumefaciens* carrying a 35S::LIMYB–GFP construct and a 35S::YFP–GmNAC81 construct. Forty-eight hours after infiltration, the subcellular localizations of the fluorescent fusion

proteins were examined by confocal microscopy. The figure shows representative confocal images from two independent experiments. **b**, Confocal fluorescence image of transiently expressed GFP (left) or LIMYB–GFP (right) in epidermal cells of tobacco leaves. Scale bars, 10 μm. The figure shows representative confocal images from two independent experiments. **c**, Immunoblotting of transiently expressed LIMYB–GFP in epidermal cells of tobacco leaves. Total protein was extracted from agro-infiltrated *N. benthamiana* leaves containing the 35S::GFP (left lanes) or 35S::LIMYB–GFP (right lanes) constructs and immunoblotted with an anti-GFP monoclonal antibody to examine the stability of the fusion protein. The positions of molecular mass are shown in kDa. **d**, Confocal fluorescence image of transiently expressed GFP–LIMYB in epidermal cells of tobacco leaves. Scale bars, 10 μm. The figure shows representative confocal images from four independent experiments. **e**, Confocal fluorescence image of transiently expressed LIMYB–GFP in epidermal cells of tobacco leaves. Scale bars, 10 μm. The figure shows representative confocal images from four independent experiments. **f**, **g**, Confocal fluorescence image of root cells stably transformed with YFP–LIMYB or LIMYB–GFP. Root tips from transgenic seedlings expressing YFP–LIMYB (**f**) or LIMYB–GFP (**g**) were directly examined under a laser confocal microscope. Scale bars, 20 μm. The figures show representative confocal images from three biological replicas. Neither the fusion of YFP to the LIMYB N terminus nor GFP to its C terminus altered the nuclear localization of LIMYB in either agro-inoculated *N. tabacum* leaves or stably transformed *Arabidopsis* roots. **h**, **i**, Confocal fluorescent image of LIMYB fused to GFP or mCherry under the control of its own promoter. The figures show representative confocal images from two independent experiments. The fluorescence was also concentrated in the nucleus of transfected cells by expression of LIMYB–GFP or LIMYB–mCherry fusions under the control of the LIMYB endogenous promoter. Scale bars, 20 μm. Collectively, these results indicate that LIMYB was localized in the nucleus.

Nature ISSN 0028-0836 EISSN 1476-4687

© 2015 Macmillan Publishers Limited. All Rights Reserved.
partner of AGORA, HINARI, OARE, INASP, ORCID, CrossRef, COUNTER and COPE

Extended Data Figure 8: *LIMYB*, *RPL10* and *NIK1* display overlapping expression profiles.

From

NIK1-mediated translation suppression functions as a plant antiviral immunity mechanism

Cristiane Zorzatto, João Paulo B. Machado, Kênia V. G. Lopes, Kelly J. T. Nascimento, Welison A. Pereira, Otávio J. B. Brustolini, Pedro A. B. Reis, Iara P. Calil, Michihito Deguchi, Gilberto Sachetto-Martins, Bianca C. Gouveia, Virgílio A. P. Loriato, Marcos A. C. Silva, Fabyano F. Silva, Anésia A. Santos, Joanne Chory & Elizabeth P. B. Fontes

Nature **520**, 679–682 (30 April 2015) doi:10.1038/nature14171

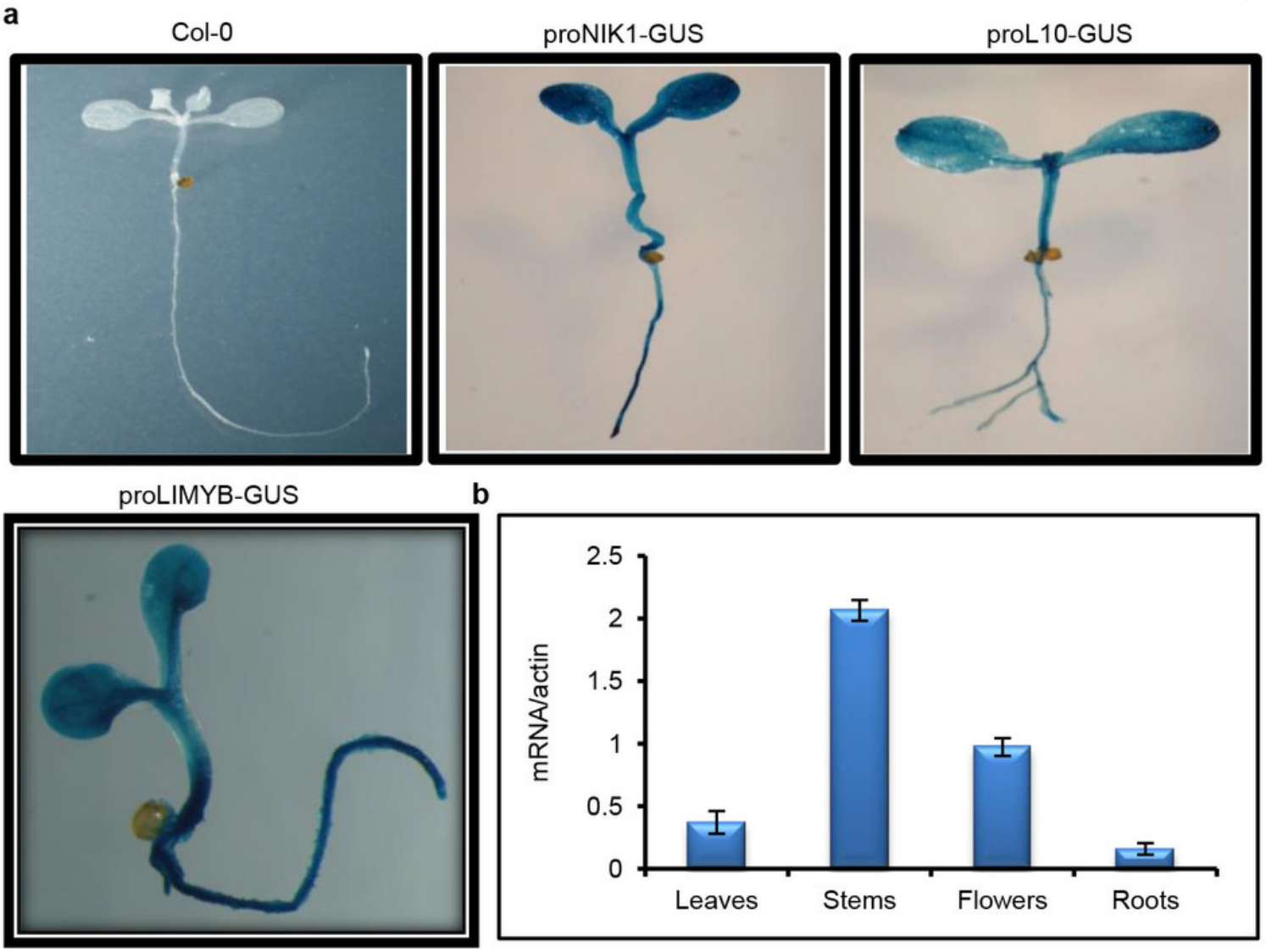

a, pLIMYB::GUS, pRPL10::GUS and pNIK1::GUS are ubiquitously expressed in seedling tissues. GUS reporter gene expression was histochemically monitored in 2-week-old seedling leaves and roots from transgenic lines harbouring a β-glucuronidase (*GUS*) reporter gene expressed from the LIMYB, RPL10 and NIK1 promoters. The figure shows representative GUS staining images of three seedlings per genotype. All three genes were ubiquitously expressed in all seedling tissues. **b**, Expression analysis of LIMYB in various plant organs. *LIMYB* expression was monitored by qRT–PCR of RNA prepared from leaves, roots, stems or flowers of Col-0 plants. Gene expression was calculated using the $2^{-\Delta Ct}$ method, and actin was used as an endogenous control. Error bars, 95% confidence intervals (n = 3) based on bootstrap resampling replicates of three independent experiments. LIMYB was also expressed in the leaves, roots, stems and flowers, indicating that *LIMYB*, *RPL10* and *NIK1* are co-expressed in several organs.

Nature ISSN 0028-0836 EISSN 1476-4687

© 2015 Macmillan Publishers Limited. All Rights Reserved.
partner of AGORA, HINARI, OARE, INASP, ORCID, CrossRef, COUNTER and COPE

Extended Data Figure 9: Controls for the regulation of RP gene expression experiments.

From

NIK1-mediated translation suppression functions as a plant antiviral immunity mechanism

Cristiane Zorzatto, João Paulo B. Machado, Kênia V. G. Lopes, Kelly J. T. Nascimento, Welison A. Pereira, Otávio J. B. Brustolini, Pedro A. B. Reis, Iara P. Calil, Michihito Deguchi, Gilberto Sachetto-Martins, Bianca C. Gouveia, Virgílio A. P. Loriato, Marcos A. C. Silva, Fabyano F. Silva, Anésia A. Santos, Joanne Chory & Elizabeth P. B. Fontes

Nature **520**, 679–682 (30 April 2015) doi:10.1038/nature14171

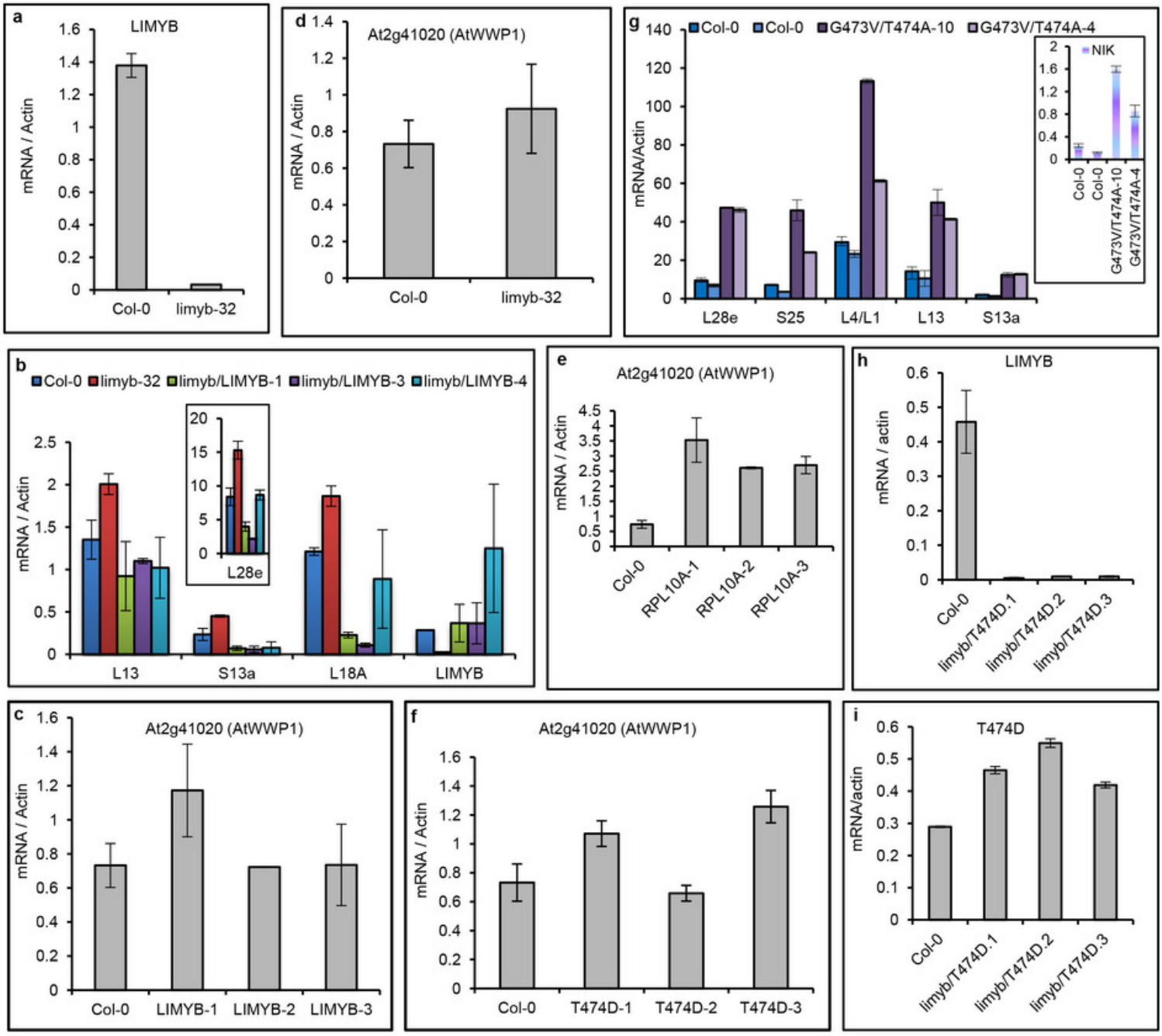

a–**i**, Expression of the indicated genes in the leaves of independent transgenic lines was monitored by qRT–PCR. **a**, *LIMYB* expression in the *limyb-32* mutant was examined. **b**, *LIMYB* expression in *limyb-32* mutant restores wild-type expression of the RP genes. Expression of the *S13a*, *L18A* and *L28e* genes was

monitored in three independently transformed *limyb-32* knockout plants with the *LIMYB* gene. **c**–**f**, Expression of the unrelated gene *AtWWP1* was monitored as a negative control in three independently transformed *LIMYB*-, *RPL10*- and T474D-overexpressing lines in addition to the *limyb-32* mutant. **g**, The double-mutant inactive kinase, G4743V/T474A, does not downregulate the RP genes. The transcript accumulation of the indicated RP genes was quantified by qRT–PCR in two independently transformed *nik1* knockout lines expressing the G4743V/T474A double mutant. **h**, **i**, Expression of *LIMYB* (**h**) and the transgene T474D (**i**) was monitored in the *limyb-32* lines, which were transformed with T474D. **a**–**i**, Means ± 95% confidence intervals (n = 3) based on bootstrap resampling replicates of three independent experiments are shown.

Nature ISSN 0028-0836 EISSN 1476-4687

© 2015 Macmillan Publishers Limited. All Rights Reserved.
partner of AGORA, HINARI, OARE, INASP, ORCID, CrossRef, COUNTER and COPE

Extended Data Figure 10: T474D requires LIMYB function to mediate the downregulation of translational machinery-related genes.

From

NIK1-mediated translation suppression functions as a plant antiviral immunity mechanism

Cristiane Zorzatto, João Paulo B. Machado, Kênia V. G. Lopes, Kelly J. T. Nascimento, Welison A. Pereira, Otávio J. B. Brustolini, Pedro A. B. Reis, Iara P. Calil, Michihito Deguchi, Gilberto Sachetto-Martins, Bianca C. Gouveia, Virgílio A. P. Loriato, Marcos A. C. Silva, Fabyano F. Silva, Anésia A. Santos, Joanne Chory & Elizabeth P. B. Fontes

Nature **520**, 679–682 (30 April 2015) doi:10.1038/nature14171

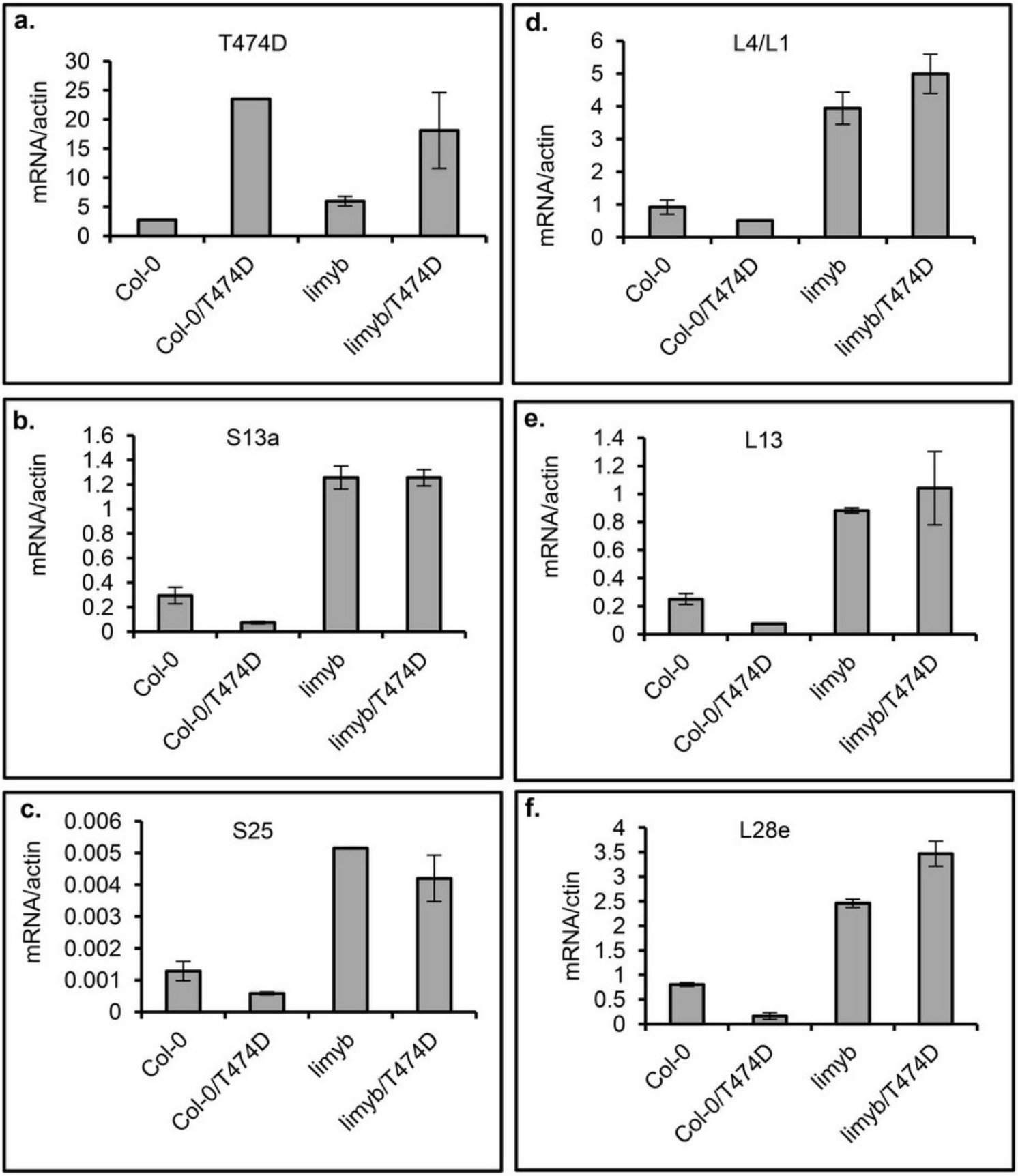

a–**f**, A 35S::T474D–GFP construct was electroporated into protoplasts prepared from Col-0 and *limyb-32* seedlings, and the expression of the indicated RP genes was monitored by qRT–PCR of RNA prepared from untransfected and transfected protoplasts. Gene expression was calculated using the $2^{-\Delta Ct}$ method, and actin and ubiquitin were used as an endogenous control. Means ± 95% confidence intervals (n = 3) based on bootstrap resampling replicates of three independent experiments are shown.

Nature ISSN 0028-0836 EISSN 1476-4687

© 2015 Macmillan Publishers Limited. All Rights Reserved.
partner of AGORA, HINARI, OARE, INASP, ORCID, CrossRef, COUNTER and COPE